The Plant Cell, Vol. 26: 3728–3744, September 2014, www.plantcell.org

Spatio-Temporal Dynamics of Fructan Metabolism in Developing Barley Grains[W]

Manuela Peukert,[a] Johannes Thiel,[a] Darin Peshev,[b] Winfriede Weschke,[a] Wim Van den Ende,[b] Hans-Peter Mock,[a] and Andrea Matros[a,1]

[a] Leibniz Institute of Plant Genetics and Crop Plant Research, D-06466 Stadt Seeland, OT Gatersleben, Germany
[b] Lab of Molecular Plant Biology, Institute of Botany and Microbiology, KU Leuven, B-3001 Leuven-Heverlee (2434), Belgium

Barley (*Hordeum vulgare*) grain development follows a series of defined morphological and physiological stages and depends on the supply of assimilates (mainly sucrose) from the mother plant. Here, spatio-temporal patterns of sugar distributions were investigated by mass spectrometric imaging, targeted metabolite analyses, and transcript profiling of microdissected grain tissues. Distinct spatio-temporal sugar balances were observed, which may relate to differentiation and grain filling processes. Notably, various types of oligofructans showed specific distribution patterns. Levan- and graminan-type oligofructans were synthesized in the cellularized endosperm prior to the commencement of starch biosynthesis, while during the storage phase, inulin-type oligofructans accumulated to a high concentration in and around the nascent endosperm cavity. In the shrunken endosperm mutant *seg8*, with a decreased sucrose flux toward the endosperm, fructan accumulation was impaired. The tight partitioning of oligofructan biosynthesis hints at distinct functions of the various fructan types in the young endosperm prior to starch accumulation and in the endosperm transfer cells that accomplish the assimilate supply toward the endosperm at the storage phase.

INTRODUCTION

Grain development comprises complex regulatory pathways that control the evolution and degeneration of tissues and the bulk accumulation of storage compounds. During the storage phase (Figure 1A), which occurs in barley (*Hordeum vulgare*) during the first 6 d after pollination (DAP), the endosperm cellularizes (Olsen, 2001; Weschke et al., 2003). The nucellus undergoes programmed cell death (PCD) except in the portion adjacent to the main vascular bundle, which differentiates into the nucellar projection (NP). In parallel, the region of the syncytium abutting the NP begins to cellularize and to differentiate into the endosperm transfer cells (ETCs) (Thiel et al., 2012). The transition phase (6 to 8 DAP) is characterized by transcriptional and physiological reprogramming, involving the expression of a suite of genes related to energy production and storage product synthesis (Sreenivasulu et al., 2004; Wobus et al., 2005). The composition of the mature grain is established during the storage phase (9 to 23 DAP). Grain filling relies on an unhampered import of assimilate from the mother plant, mainly in the form of sucrose, channeled from the vascular bundle via cells of the ventral crease into the endosperm. The NP and ETCs represent the maternal-filial boundary and control the assimilate transfer toward the endosperm (Wang et al., 1995a; Offler et al., 2003). At the beginning of the storage phase, a large apoplastic gap (the endosperm cavity) emerges between the NP and ETCs (Figure 1B), and the morphology of the cells facing this cavity has been shown to resemble that of transfer cells (Weschke et al., 2000; Patrick and Offler, 2001). The many morphological features emphasize the complexity of the physiological processes occurring in these cells and more generally the process of grain filling.

In current models, the maintenance of sink strength during grain filling depends on the cleavage of sucrose by invertases and sucrose synthase. Invertases are also important for the production of hexose sugar signals that regulate cell cycle and cell division programs (Koch, 2004; Bihmidine et al., 2013). Certain aspects of development are regulated by the sucrose-to-hexose ratio, as shown for cell division events during tuber, embryo, and root growth (Weber et al., 1997; Roessner-Tunali et al., 2003; Wind et al., 2010). The same ratio also affects various other physiological processes, such as the synthesis of primary (plastocyanin and patatin) and secondary (anthocyanins) metabolites and transporter gene transcription (Wind et al., 2010). The regulatory network involving sugars during the development of the cereal grain is far from being completely understood. In the barley grain, the hexose content of filial tissues is highest during the prestorage phase, accompanied by the localized transcription of a cell wall invertase in ETCs (Weschke et al., 2000). When storage product synthesis starts, the levels of hexoses drop and the activity of sucrose synthase increases dramatically (Weschke et al., 2000); simultaneously, cellularization ceases in the endosperm (Wobus et al., 2005).

Details of metabolic activity in the developing barley grain are now emerging due to methodologies that allow resolving down to the cellular level. Laser microdissection (LM) of barley grain tissues has facilitated the recognition of various signal transduction pathways regulating primary metabolism and defense reactions active in the NP and ETCs (Thiel et al., 2008). Some

[1] Address correspondence to matros@ipk-gatersleben.de.
The author responsible for distribution of materials integral to the findings presented in this article in accordance with the policy described in the Instructions for Authors (www.plantcell.org) is: Andrea Matros (matros@ipk-gatersleben.de).
[W] Online version contains Web-only data.
www.plantcell.org/cgi/doi/10.1105/tpc.114.130211

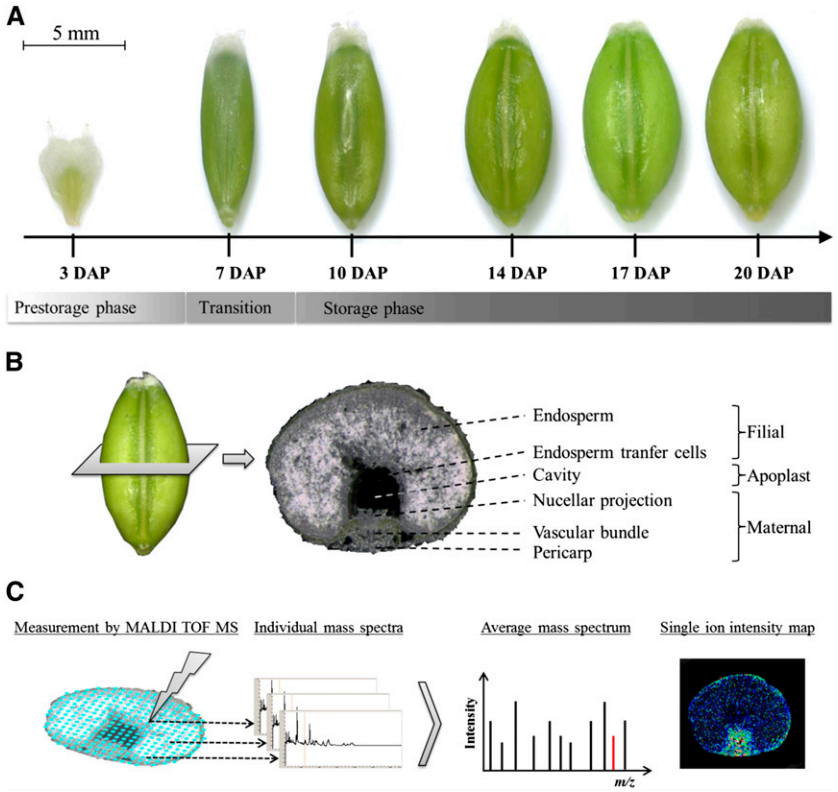

Figure 1. Schematic Representation of the Experimental Setup for Analysis of Metabolite Distribution Patterns by Mass Spectrometry Based Imaging.

(A) The developmental stages of the barley grain.
(B) A cross section of a 14 DAP barley grain along with the annotation of the most relevant grain tissues. For preparation of cross sections (30 µm), frozen grains were fixed on the sample holder of a cryotome.
(C) Acquisition of mass spectrometric data by randomized measurement of individual laser raster spots. Individual spectra are summarized to an average mass spectrum for peak detection and visualization of peak intensities by ion intensity maps; exemplarily illustrated for the red peak indicating an *m/z* of 448.2

correlations have been established between transcriptional activity and metabolite concentration in the NP and ETCs of barley grains (Thiel et al., 2009). Studies on the metabolic compartmentation within developing barley grains so far showed local variation in endospermal sucrose and alanine concentration (Melkus et al., 2011; Rolletschek et al., 2011), which might be correlated to uneven levels of hypoxia within the grain (Rolletschek et al., 2004). Although it has long been known that fructosyl oligosaccharides are enriched in the endosperm cavity of the wheat (*Triticum aestivum*) grain during late storage (20 to 27 DAP) (Ugalde and Jenner, 1990; Schnyder et al., 1993), their role in grain development remains unclear. Fructans are a recognized constituent of cereal grains of different species (Henry and Saini, 1989); they also feature in vegetative tissues and have been implicated in carbohydrate partitioning, short or longer term storage (Nelson and Spollen, 1987; Schnyder et al., 1993), and stress protection (Valluru and Van den Ende, 2008; Livingston et al., 2009). In the grain, the presence of fructans has been associated with both sucrose phloem unloading (Pollock and Cairns, 1999; De Gara et al., 2003) and osmoregulation during cell expansion and growth (Schnyder et al., 1993). Verspreet et al. (2013b) propose a role for wheat grain fructans in reactive oxygen species (ROS) detoxification related to cell division processes during prestorage.

The formation of secondary cell walls in ETCs and the NP, along with enhanced transport activity and PCD in the central part of the NP are accompanied by the upregulation of genes and gene products related to ROS scavenging in the ETC (Thiel et al., 2008; Kaspar et al., 2010; Thiel et al., 2012). The importance of ETCs for grain yield has been shown in several studies (Weschke et al., 2000, 2003; Weber et al., 2005). However, the machinery responsible for the protection of the ETCs, and hence the maintenance of assimilate transport into the endosperm, has not been elucidated as yet.

Here, we describe the distribution of oligosaccharides in time and space and relate this to endosperm formation and grain filling. Detailed analysis of sugar extracts specified structural fructan isomers during the prestorage and the storage phase. At the same time, we deduced the transcription profiles of various genes active in the fructan biosynthesis pathway by sampling specific microdissected grain tissues. We observed a high accumulation of inulin-type oligofructans in and around the emerging endosperm cavity during the storage phase, whereas the graminan- and levan-type oligofructans accumulated prior to

storage product biosynthesis in the cellularized endosperm. We also analyzed grains of the *seg8* endosperm mutant (Felker et al., 1985) impaired in the differentiation of transfer tissues and, accordingly, in sucrose import toward the endosperm (Melkus et al., 2011). Because sucrose is a direct precursor for the production of fructosyl oligosaccharides, characteristic fructan distribution patterns are not established in mutant grains. We hypothesize that the remarkable partitioning of fructan biosynthesis relates to different functions of the various oligofructan types in the young endosperm prior to starch accumulation and in the ETCs that actively transfer solutes toward the endosperm at the storage phase.

RESULTS

Oligosaccharide Distribution Patterns Are Tissue and Developmental Stage Dependent

Grains were sampled at the prestorage (3 DAP), transition (7 DAP), and storage phase (10 to 20 DAP) (Figure 1A). The matrix-assisted laser desorption/ionization (MALDI) mass spectrometry imaging (MSI) technique allows the visualization of oligosaccharides in grain tissues with a lateral resolution of 30 µm. It was possible to distinguish hexose polymers up to a degree of polymerization (DP) of seven. The sugars were identified according to their typical fragmentation pattern, displaying neutral losses of *m/z* 162 (Supplemental Figure 1). A full list of the molecular ions detected in our study is provided in Table 1.

During the prestorage phase, a generally higher abundance of DP 4-7 oligosaccharides in the pericarp was observed (Figure 2; Supplemental Figure 2). By 7 DAP, sugars had become uniformly distributed across the grain, but once the switch to the storage phase had occurred, distinctive patterns of oligosaccharide accumulation began to develop. Tri- and tetrasaccharides accumulated around the nascent endosperm cavity (Figure 2C; Supplemental Figures 2B and 3). An alignment of the MSI data with histological sections indicated that the highest concentration of these sugars was present in the tissues bordering the cavity, a pattern that persisted until the end of the grain filling period. In contrast, DP 5-7 oligosaccharides accumulated preferentially in the central endosperm (Figure 2D; Supplemental Figures 2C, 2D, and 3).

Table 1. Sugar Molecular Ions Detected by Means of MALDI MSI

Sugar Molecule	Chemical Formula	Molecular Ions Generated in MALDI TOF and ESI TOF Mass Spectrometry		
		$[M+H]^+$	$[M+Na]^+$	$[M+K]^+$
Hexose	$C_6H_{12}O_6$	181.1	203.1	219.0
Disaccharide	$C_{12}H_{22}O_{11}$	343.1	365.1	381.1
Trisaccharide	$C_{18}H_{32}O_{16}$	505.2	527.2	543.1
Tetrasaccharide	$C_{24}H_{42}O_{21}$	667.2	689.2	705.2
Pentasaccharide	$C_{30}H_{52}O_{26}$	829.3	851.3	867.2
Hexasaccharide	$C_{36}H_{62}O_{31}$	991.3	1013.3	1029.3
Heptasaccharide	$C_{42}H_{72}O_{36}$	1153.4	1175.4	1191.3

By using DHB as matrix, a major detection of the sugar potassium adducts $[M+K]^+$ was revealed, followed by the detection of the sodium adducts $[M+Na]^+$. The protonated $[M+H]^+$ ions were not detected (please also refer to Supplemental Figure 1).

The Differentially Accumulated Oligosaccharides Are Oligofructans

Sucrose is a direct precursor for the production of both fructosyl and galactosyl oligosaccharides. Both compound classes are known to be present in cereal grains (Henry and Saini, 1989; Verspreet et al., 2013b). As we detected pronounced reallocation of the various oligosaccharides during the shift from the prestorage to the storage phase, we identified the hexose moieties of sugars by enzymatic reactions.

The treatment of extracted cavity sap with α-galactosidase generated no novel products, while reaction with fructan 1-exohydrolase (1-FEH) led to the degradation of cavity sap oligosaccharides to sucrose and fructose monomers (Supplemental Figure 4). Invertases (INVs) split sucrose into its constituent hexoses and are also capable of cleaving small fructan molecules (Verspreet et al., 2013a). To validate the distribution of individual sugars, on-tissue digestion with INV was performed and followed by MSI analysis, along with a nontreated control to ensure direct comparability of signal intensities (Figure 3). The resulting MSI data revealed a high abundance of oligofructans in the endosperm cavity, as shown by a massive decline in the relevant molecular ion signals (Figure 3B). The trisaccharide molecular ion (*m/z* 543) signal in particular was very strongly depleted in the cavity region, as also observed from the corresponding ion intensity maps (Figure 3C, right panel), while that for hexoses (*m/z* 219) was increased (Figure 3C, left panel). The on-tissue INV enzyme assay also confirmed sucrose as the predominant disaccharide (*m/z* 381) discernible from the decreased sucrose signal in the spectrum as well as from the ion intensity map below. The remaining disaccharide in the endosperm (Figure 3C, middle panel) may be maltose, which is not degraded by INV; its concentration was similar to that of sucrose at 14 DAP (Supplemental Table 1).

Our results revealed oligofructan accumulation during the storage phase in the endosperm cavity, with highest signal intensities in cell layers surrounding this cavity.

1-Kestose and Nystose Accumulate in the Endosperm Cavity during the Storage Phase

To gain further information on spatio-temporal differences in individual fructan concentrations, we analyzed endosperm cavity extracts and total grains at different developmental stages. At 7 DAP, the cavity had not yet been formed, thus sugars were extracted from the manually dissected NP region. The individual sugar concentrations in the cavity were compared with those in total grains (Figure 4). Glucose and fructose concentrations were found to peak before the onset of massive starch biosynthesis (7 DAP), and a 3- to 4-fold decline in the hexose concentration took place between 7 and 10 DAP (Figure 4A). This was detected both from intact grains and from cavity extracts and thereby is in agreement with the general finding that the prestorage phase is characterized by a higher hexose-to-sucrose ratio (Figure 4B).

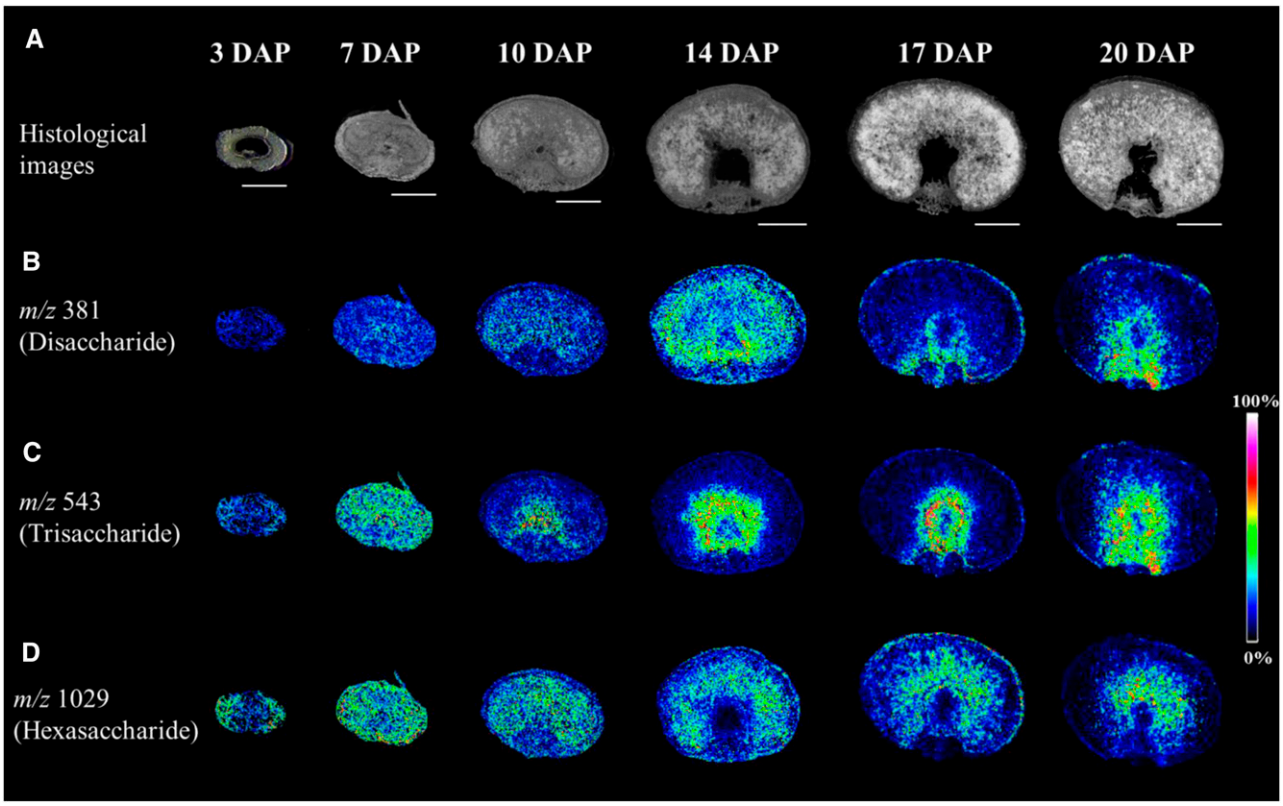

Figure 2. Accumulation Patterns of Oligosaccharides during Barley Grain Development as Observed by MALDI MSI.

(A) Histological images illustrating the various developmental stages sampled.
(B) The distribution of the disaccharide (*m/z* of 381).
(C) Ion intensity maps of the trisaccharide (*m/z* 543). Specific accumulation in and around the nascent endosperm cavity was observed from 10 DAP onwards.
(D) The hexasaccharides (*m/z* 1029), which accumulated in the pericarp during the prestorage phase (3 DAP), moved to the endosperm at the beginning of the storage phase (from 10 DAP onwards). Bars = 1 mm.

Hexose concentrations declined strongly (~3-fold) during linear starch accumulation (10 to 20 DAP) in the total grain extracts, while in the cavity extracts, glucose concentration significantly increased from 14 to 20 DAP (2.3-fold; $P = 0.012$), whereas that of fructose did not change significantly. The sucrose concentration declined by 1.7-fold from 7 to 10 DAP, which was less steep compared with hexoses. During the storage phase, the sucrose concentration was 2.1- to 2.8-fold higher in the endosperm cavity than in the whole grain (Figure 4B). The maltose concentration of the whole grain declined over the period 10 to 14 DAP but increased between 17 and 20 DAP. Maltose was not detectable in the cavity extracts (Supplemental Table 1) in agreement with the MALDI MSI-based analysis (Figure 3C). Quantification of the fructan molecules confirmed the data obtained by MALDI MSI. There was a strong increase in the cavity sap content of both the inulin-type fructans 1-kestose (2.8-fold; $P \leq 0.001$) and nystose (2.0-fold; $P = 0.004$) between 10 and 20 DAP (Figure 4C), whereas their concentration in the whole grain barely changed over this period. The concentrations of 6-kestose (DP 3) and bifurcose (DP 4) fell by ~2- to 5-fold ($P \leq 0.001$) after the switch to the storage phase, both in the cavity sap and in the whole grain (Figure 4C).

The observed temporal and tissue-specific oligofructan accumulation patterns point to a tight regulation of fructan metabolism.

The Transcription of Fructan Biosynthesis Encoding Genes Is Tissue and Development Specific

1-Kestose and nystose belong to inulin-type fructans for which β(2,1) linkages of the fructosyl moieties are characteristic. Their biosynthesis is catalyzed by the activity of sucrose:sucrose 1-fructosyltransferase (1-SST) and fructan:fructan 1-fructosyltransferase (1-FFT). The formation of β(2,6) linkages between the fructose moieties is catalyzed by the sucrose:fructan 6-fructosyltransferase (6-SFT) forming levan and graminan types of fructans. The fructose in 6-kestose is linked to sucrose by a β(2,6) linkage and bifurcose consists of a β(2,6) linked fructose to 1-kestose (Figure 4D).

The transcript abundances of genes encoding fructan metabolism enzymes were obtained by quantitative RT-PCR (qRT-PCR), based on templates extracted from LM grain tissues (the NP, ETCs, and the wings and central part of the endosperm; see Figure 5A) sampled between 5 and 14 DAP. The gene encoding

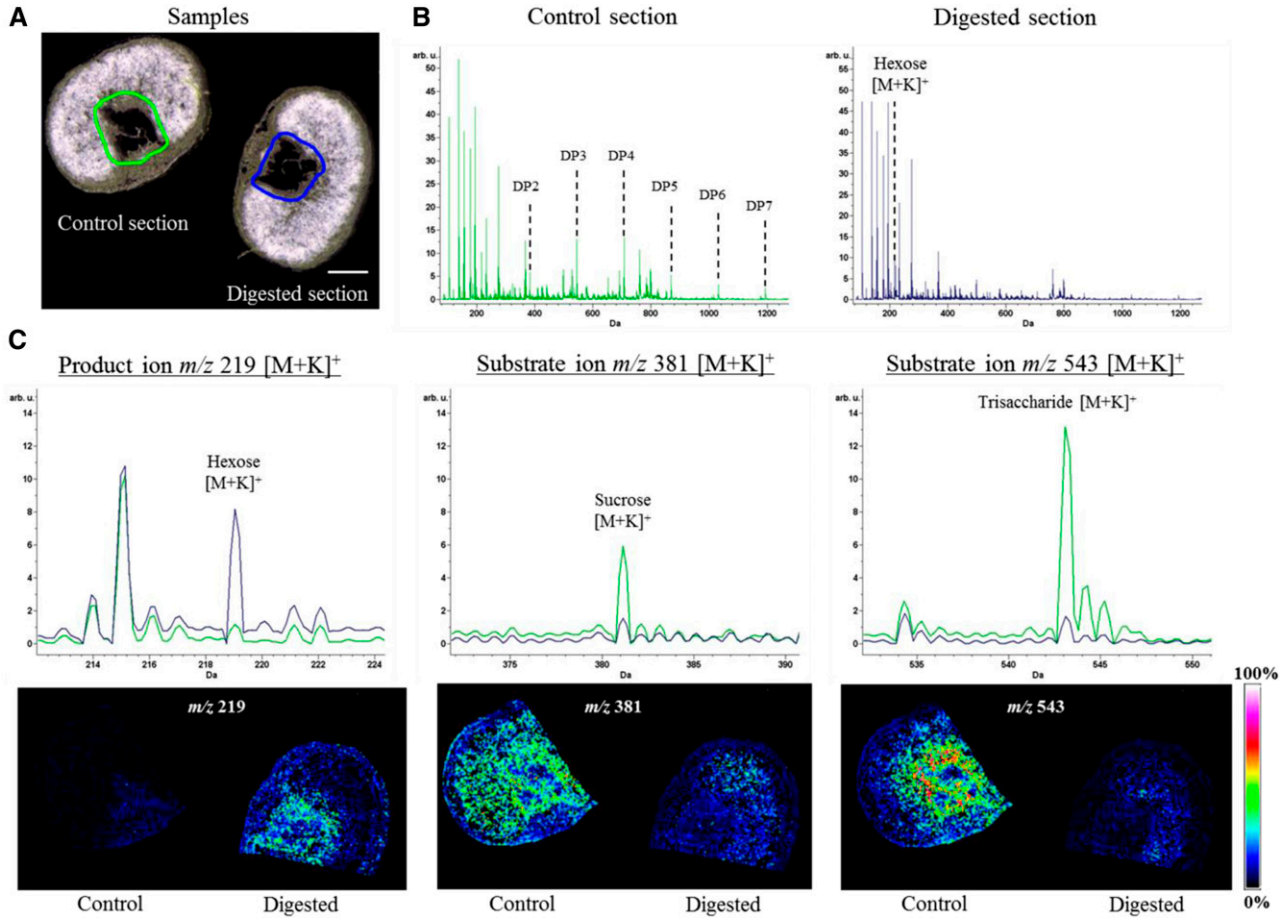

Figure 3. Spatially Resolved On-Tissue Digestion and Subsequent MSI Analysis.

Cryosections were treated with either yeast invertase or buffer as a control. Subsequently, sections were analyzed by MALDI MSI.
(A) Histological images of sections used for digestion experiments. Bar = 1 mm.
(B) Average spectra of sample sections (indicated in **[A]** by green [control] and blue [digested]). The control section shows the full complement of sugars (DP 2-7), which was not obtained from the digested section. Here, the hexose peak is most abundant from the sugar signals.
(C) Enlargements of the spectra overlay from the control and the digested section, displaying the signal for the hexose product ion (*m/z* 219) and the substrates sucrose (*m/z* 381) and trisaccharide (*m/z* 543). The corresponding MSI results are illustrated below each spectrum. Colors used in the single ion intensity maps correspond to signal intensities displayed at the right.

1-SST that catalyzes 1-kestose production, which is required as acceptor substrate of both 6-SFT and 1-FFT (Figure 4D), was strongly expressed in the endosperm (particularly in its peripheral region) at 5 DAP (Figure 5B). At 7 DAP, the peak of transcript abundance changed to the mitotically active region of the NP. The strongest observed transcription of 1-SST was found in the NP region at 10 DAP, while at later stages the expression level diminished (Supplemental Table 2). Transcription of the gene encoding 1-FFT (which catalyzes the elongation of 1-kestose to generate nystose; see Figure 4D) was restricted to the NP, with its peak of abundance occurring at 10 DAP in the upper part of the NP (Figure 5B).

The gene expression patterns of 1-SST and 1-FFT correspond to the accumulation of 1-kestose and nystose at the start of the storage phase. In contrast, the level of 6-SFT transcript was high in the endosperm at 5 DAP, when the endosperm underwent cellularization and before starch biosynthesis started. A low level of transcription was observed for this gene in the NP and ETCs (Figure 5B). The fall in 6-SFT transcription at 10 DAP mirrored the observed decline in the concentrations of 6-kestose and bifurcose (Figure 4C).

Among the fructan degrading enzymes, transcripts of the gene encoding 1-FEH were most abundant at 10 DAP in the upper part of the NP, that region where synthesis of 1-kestose and nystose is thought to take place. Transcript levels were very low at 5 DAP throughout the grain (Supplemental Table 2) and ceased by 14 DAP (Figure 5C). Simultaneous gene expression of biosynthesis and catabolism enzymes of inulin-type fructans indicates a stimulated metabolism of this group of oligofructans and might hint to an adaptation of chain length for optimal functionality. No fructan 6-exohydrolase transcripts were observed, the enzyme involved in degradation of 6-kestose (Figure 4D).

Transcriptional activities of fructan biosynthesis genes in distinct endosperm tissues indicate de novo biosynthesis of levan- and graminan-type fructans from sucrose at the prestorage

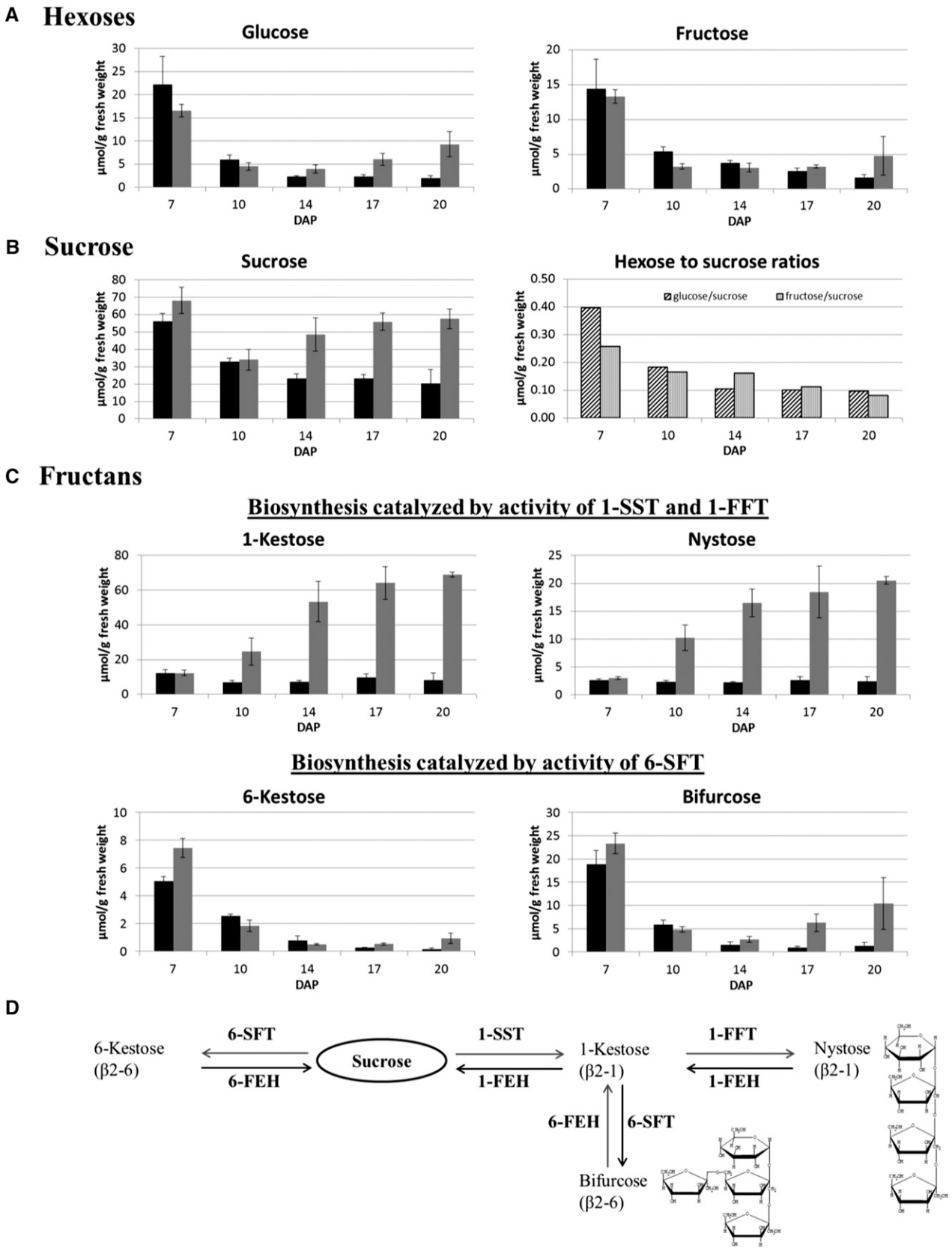

Figure 4. Quantification of Sugars Present in the Developing Barley Grain.

Concentrations of sugars in the isolated transfer region (7 DAP, gray bars) and cavity extracts (10 to 20 DAP, gray bars) are compared with those obtained for whole grains (black bars). Raffinose has not been detected at the investigated developmental stages. Levels of maltose are given in Supplemental Table 1.

phase until onset of grain filling. During grain filling, substantial de novo biosynthesis of inulin-type fructans can be concluded to take place in the NP. The gene expression studies coincide with distribution patterns of oligosaccharides and concentrations of the different oligofructan types in the cavity sap. These conclusions are further supported by the identification of 6-SFT (for which highest amounts of transcripts have been detected in the endosperm) in protein extracts of dissected transfer region and endosperm at 7 and 10 DAP (Supplemental Figure 5).

Fructan Distribution Patterns Are Not Established in *seg8* Mutant Grains

The correlation between fructan distribution patterns and alterations in cellular differentiation during grain development has been investigated in the maternally affected shrunken endosperm mutant *seg8* (Felker et al., 1985) with a yet unknown primary gene defect. Grains of the wild-type variety 'Bowman' and *seg8* were sampled at the early storage phase (10 to 14 DAP) and sugar distribution patterns were analyzed by MALDI MSI. The tissue- and developmental stage-dependent oligosaccharide distribution patterns observed for 'Bowman' resemble those of 'Barke' (see above). Partitioning of sucrose is changed in the *seg8* endosperm in comparison to 'Bowman', whereas DP 5-7 oligosaccharides accumulate in the ventral pericarp in *seg8* but in the endosperm in 'Bowman' (Supplemental Figure 6). At 10 DAP, DP 3 (Figure 6) and DP 4 (Supplemental Figure 6) oligosaccharides, namely, fructans, start to accumulate in the tissues around the nascent endosperm cavity in 'Bowman'. In contrast, fructans (DP 3 *m/z* 534 and DP 4 *m/z* 705) were barely detectable around this region in *seg8* grains, indicating that the characteristic distribution pattern has not been established in mutant grains (Figure 6; Supplemental Figure 6).

The transcript abundances of genes encoding fructan metabolism enzymes in the var Bowman tightly correlated to those of 'Barke' (Supplemental Table 3), with a maximum of 1-SST transcription in the endosperm wings at 5 DAP, of 1-FFT in the NP region at 7 DAP, of 6-SFT throughout the endosperm at 5 DAP, and of 1-FEH in the NP region and ETC at 7 to 10 DAP. Gene activity was compromised in *seg8*. Remarkably, the transcription of 1-SST and 6-SFT was strongly reduced in the endosperm at 5 DAP and transcripts of 1-FFT and the degrading enzyme 1-FEH were not detectable in the NP of *seg8* at 7 and 10 DAP, respectively. This indicates that disturbances of proper differentiation of the transfer tissues NP and ETCs strongly impact fructan biosynthesis in both maternal NP and developing endosperm.

Oligosaccharides React with Hydroxyl Radicals

The ETCs and parts of the NP depict transfer cell morphology (Weschke et al., 2000; Thiel et al., 2012). Cells that actively mediate transport processes produce substantial quantities of ROS (Luthje et al., 2013). The hydroxyl radical ($^{\bullet}$OH), thought to be the most reactive ROS (Van Breusegem and Dat, 2006; Gadjev et al., 2008), is formed by the Fenton reaction from hydrogen peroxide (Figure 7B; Fenton, 1894). The interaction of sugars with the hydroxyl radical is thought to involve a hydrogen transfer from a sugar C-H bond (Hernandez-Marin and Martínez, 2012). The resulting sugar radicals break down into a radical and a nonradical product (Peshev et al., 2013) or react with gaseous oxygen and form oxidized oligosaccharides (Supplemental Figure 7B; Von Sonntag and Schuchmann, 2001).

The scavenging capacity of fructan oligomers was studied in in vitro Fenton reactions using extracted cavity sap. We observed the degradation of the oligosaccharides, especially of the DP 4-7 oligosaccharides. DP 2-7 molecules can be recognized by their sodium adducts (Figures 7A and 7D). The molecular ion abundance of oligosaccharides of higher DP was substantially reduced by the reaction, thus shifting the ratio to higher levels of mono- and disaccharides (Figure 7B).

The mass spectra obtained from the cavity sap indicated the presence of oxidation products for a number of oligosaccharides, recognized by a molecular ion signal at 2 D smaller than the precursor ion (Figure 7C, upper panel, and Figure 7D). Examples of these are shown for DP2 (*m/z* 363.1 $[M\text{-}2H+Na]^+$) and DP4 (*m/z* 687.2 $[M\text{-}2H+Na]^+$) (Figure 7C). The molecular ion intensity of the oxidation products was clearly enhanced when the cavity sap sample was treated with the Fenton reagent (Figure 7C, lower panel). Also, MS fragmentation of the *m/z* 525.2 compound generated both an *m/z* 365.1 ($[DP2+Na]^+$) and an *m/z* 203.1 ($[DP1+Na]^+$) peak, confirming that the *m/z* 525.2 peak originated from an oligosaccharide (Supplemental Figure 7). Collectively, the reactivity of sugar oligomers, in particular of fructans, with hydroxyl radicals was confirmed.

DISCUSSION

Distinct Patterns of Oligosaccharide Distribution in the Developing Barley Grain

At 3 DAP, the endosperm consists of a fluid-filled cavity surrounded by the coenocyte and the highest concentration of sugars was detected in the pericarp (Figure 2). Similarly, water-soluble carbohydrates accumulate in the pericarp of the very young wheat grain (Housley and Pollock, 1993; Schnyder et al.,

Figure 4. (continued).

(A) Concentrations of the hexoses glucose and fructose.

(B) Concentration of sucrose together with the hexose/sucrose ratios.

(C) Concentrations of oligofructans: The inulin-type fructans 1-kestose and nystose are shown in the upper diagrams and the levan-type fructans 6-kestose and bifurcose are presented in the lower diagrams.

(D) Enzymatic pathways involved in oligofructan metabolism. Sucrose is the precursor of fructan biosynthesis; it is used by 1-SST or 6-SFT to produce either inulin- or levan-type fructans, which differ in their linkages with fructose moieties (β2-1 or β2-6). Bifurcose is a mixed type containing one β2-1 and one β2-6 linkage. Mean values ± SD are shown from $n = 3$ replicates from independent sowings.

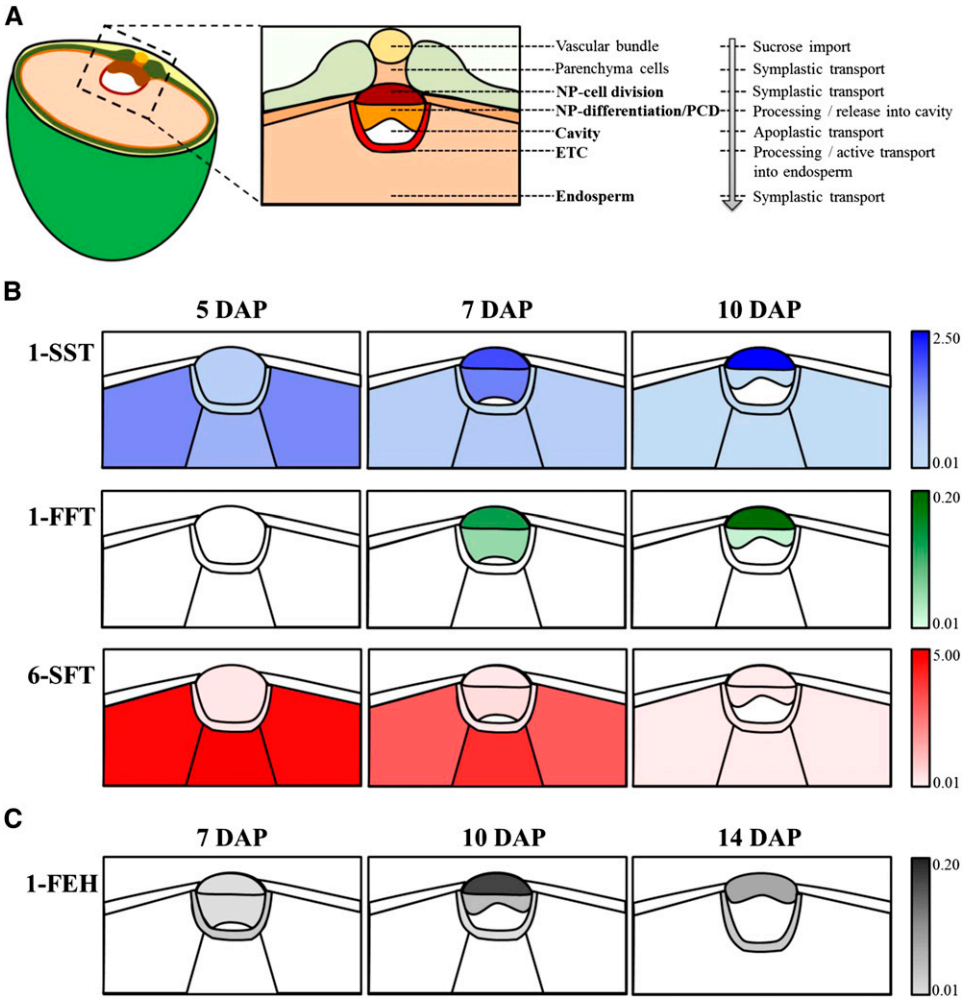

Figure 5. Graphical Representation of the Transcription Profiles of Genes Involved in Fructan Metabolism in Separated Grain Tissues.

(A) Scheme of a half-sectioned barley grain at storage stage with enlargement of tissues responsible for nutrient transfer into the endosperm. Those shown in bold lettering were analyzed by qRT-PCR using a cDNA collection from laser microdissected grain tissues. After differentiation, the NP displays a heterogeneous tissue with dividing cells in the upper part and elongating cells that partly undergo autolysis. Subsequently, from 7 to 10 DAP, both parts were divided, whereas at 14 DAP, cells of the NP were taken as a whole due to diminishing of the tissue. The endosperm has been divided into the central and the wing parts.

(B) Transcription profiles of the genes encoding biosynthetic enzymes of inulin- (1-SST, blue, and 1-FFT, green) and levan-type (6-SFT, red) fructans.

(C) Transcription profile of the gene encoding 1-FEH.

1993). Later (by 7 DAP), the disintegration of the pericarp is accompanied by a reduction of the overall water-soluble carbohydrate content and a reallocation of all detected sugars (DP 2-7). Grain filling initiation was accompanied with increasing DP 3 and 4 oligofructan levels (Figure 3), known to be present in the cereal grain (Henry and Saini, 1989; Verspreet et al., 2013b). Larger amounts of fructosyl oligosaccharides are also present in the wheat endosperm cavity at 20 to 27 DAP (Ugalde and Jenner, 1990; Schnyder et al., 1993). Here, the visualization by MSI showed that these molecules were associated with the NP and ETCs, rather than being within the cavity itself (Figure 2). Both tissues are responsible for the high import rates of assimilates into the endosperm. The concomitant decreased hexose/sucrose ratio indicates a shift toward sucrose-specific signaling processes that are known to stimulate fructan biosynthesis (Van den Ende, 2013) and are closely linked to cellular ROS homeostasis (Li et al., 2014; Van den Ende and El-Esawe, 2014).

The presence of the inulin-type molecules 1-kestose and nystose in and around the cavity rose steeply from 7 DAP onwards, but their concentration in the grain as a whole did not change appreciably over time. This behavior contrasts with that in total wheat grains, where the highest concentrations of 1-kestose and nystose have been detected before the onset of starch accumulation (Verspreet et al., 2013c). The quantities of 6-kestose and bifurcose (levan- and graminan-type) declined in both the cavity and in the whole grain, consistent with observed spatio-temporal transcript profiles of the genes encoding

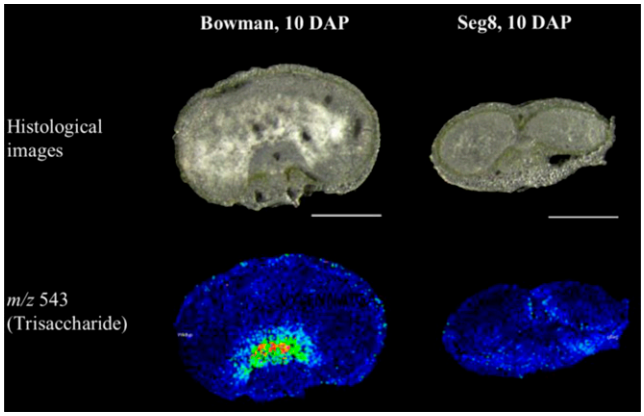

Figure 6. Accumulation Patterns of the Trisaccharide in Bowman and *seg8* as Observed by Means of MALDI MSI.

Histological images of the samples at 10 DAP (top row). Ion intensity maps of the trisaccharide (*m/z* 543, bottom row). Specific accumulation in and around the nascent endosperm cavity was observed from 10 DAP onwards for *H. vulgare* var Bowman but was not detectable in *seg8*. Bars = 1 mm.

key components of fructan metabolism. For example, the abundance of transcripts associated with the biosynthesis of inulin-type fructans (1-SST and 1-FFT) (Van den Ende et al., 2004; Livingston et al., 2009) peaked in the NP at 7 to 10 DAP. Meanwhile, the decline over development in the concentration of 6-kestose and bifurcose matched with the peak time of 6-SFT transcription and protein expression occurring in the differentiated endosperm prior to starch accumulation.

The tight correlation of regular differentiation of barley transfer tissues to fructan biosynthesis has been validated by the investigation of the *seg8* mutant. By MALDI MSI we could show that the disturbed NP development and the subsequent abnormal proliferation of the ETCs and the endosperm opposite the NP (Weier et al., 2014) is accompanied by a decreased sucrose flux toward the endosperm and a marked reduction in fructan accumulation (Figure 6). The relocation of sucrose and reduced transfer via the NP and ETCs into the endosperm of *seg8* has also been shown by in vivo NMR experiments (Melkus et al., 2011). The transcription of fructan biosynthesis genes is induced by high sucrose levels (Van den Ende, 2013); thus, a regulatory role especially for 6-SFT in maintaining the balance between hexoses and high order saccharides can be assumed (Martínez-Noël et al., 2009).

The Transient Buildup of Levan-/Graminan-Type Fructans in the Young Endosperm

Between 5 and 7 DAP, there was a major upregulation of 6-SFT in the endosperm, while at the same time, 1-SST activity would have been delivering the precursor for bifurcose biosynthesis. Hence, sucrose entering the endosperm prior to 7 DAP, which is the period when the endosperm cells are dividing and expanding, is likely to be processed partly into fructans. By 8 DAP, the barley endosperm has already established the wherewithal for starch biosynthesis resulting in strong starch accumulation until 18 DAP (Weschke et al., 2000, 2003).

One cellular role of sugars is to stimulate genes involved in growth and storage processes (while low sugar levels promote energy capture and mobilization) (Rolland et al., 2006). Thereby, hexoses and sucrose are proposed to serve as elicitors of plant sugar signaling (Wind et al., 2010). The consumption of sucrose as a result of fructosylation reactions maintains a high glucose/sucrose ratio, which in turn is required for cellularization and cell expansion in the prestorage endosperm (Weschke et al., 2003; Koch, 2004; Ishimaru et al., 2005). The activity of cell wall-bound INV is responsible for high hexose levels and mitotic activity of *Vicia faba* cotyledons (Weber et al., 1997); similarly in maize (*Zea mays*), the loss of INV activity through mutation reduces mitotic activity (Vilhar et al., 2002). A direct correlation between sucrose levels and the onset of storage product biosynthesis has been observed in the barley endosperm (Weschke et al., 2000) and the cassava (*Manihot esculenta*) tuber (Baguma et al., 2008). This appears consistent with the temporally high expression of the WRKY transcription factor SUSIBA2, a regulatory transcription factor of starch biosynthesis, and the concurrent high endogenous sucrose levels in the barley endosperm at 12 DAP (Sun et al., 2003).

An advantage of the capacity to transiently process sucrose into fructans is that both the biosynthesis and breakdown of the latter are rapid and easily accomplished (Van den Ende, 2013). It seems likely that the maintenance of a high glucose/sucrose ratio via fructan biosynthesis contributes to the proper cellularization of the young endosperm. In addition, the fructans may act as osmoregulants and thus exert control over the cell expansion process (Schnyder et al., 1993). Such regulatory function was also elaborated for cold and drought hardening (Livingston and Henson, 1998; Valluru and Van den Ende, 2008; Livingston et al., 2009).

Inulin-Type Fructans Accumulate in Transfer Cell Tissues

With the onset of starch accumulation, a switch in fructan metabolism to the biosynthesis of short-chain inulin-type fructans occurred. Inulin-type fructans appeared to be biosynthesized in the upper part of the NP and to accumulate in cells surrounding the endosperm cavity until the late storage phase (Figure 2; Supplemental Figure 2). Those cellular layers, the ETC region and parts of the NP, exhibit transfer cell morphology.

High rates of solute transport across transfer cell membranes are ensured by the orchestrated action of transporter proteins, H^+-ATPases, and cation channels (Offler et al., 2003). In the 5 to 15 DAP barley ETCs, Hv-SUT1 (encoding a sucrose/H^+ symporter) transcript is particularly abundant (Weschke et al., 2000). In control of pH and apoplastic redox state the activity of H^+-ATPase is associated with a transmembrane electron transport by NADPH-oxidases (Luthje et al., 2013), that in turn are involved in ROS production.

Although they are associated with a number of detrimental effects, ROS are also important in plant development, e.g., they have a regulatory function in establishing cell wall ingrowths in the *V. faba* cotyledon (Zhou et al., 2010; Andriunas et al., 2012). In suberin- and lignin-rich cell walls, the cross-linking of phenolics is mediated by H_2O_2 (Fry, 1998; Schweikert et al., 2000), a process that occurs in chalazal cells during the final stage of barley grain development (Cochrane, 2000; Asthir et al., 2002).

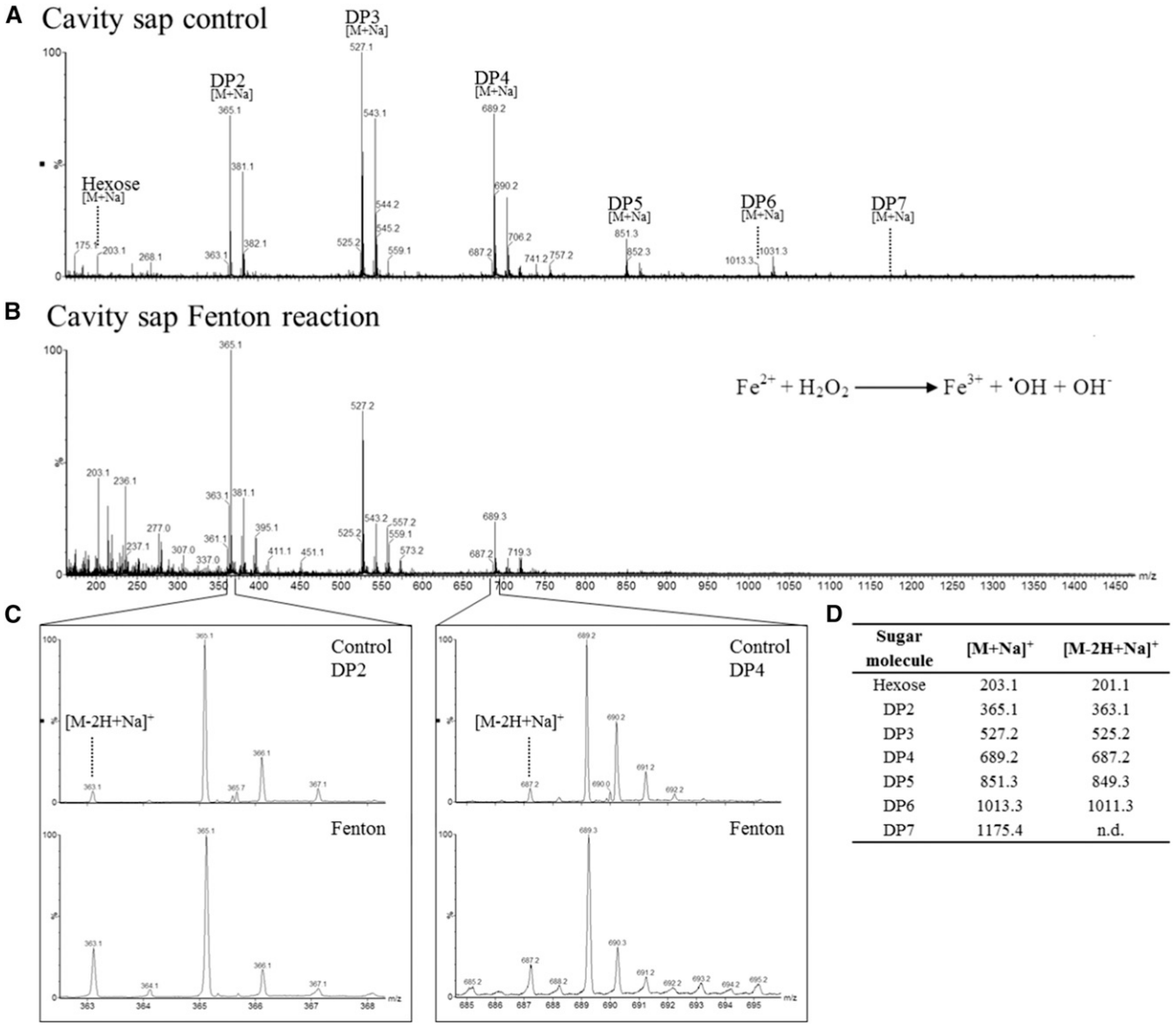

Sugar molecule	$[M+Na]^+$	$[M-2H+Na]^+$
Hexose	203.1	201.1
DP2	365.1	363.1
DP3	527.2	525.2
DP4	689.2	687.2
DP5	851.3	849.3
DP6	1013.3	1011.3
DP7	1175.4	n.d.

Figure 7. The Interaction between Sugar Oligomers and the Hydroxyl Radical.

During the Fenton reaction, a mixture of hydrogen peroxide and an iron catalyst leads to the oxidation of organic compounds, which is accompanied by the generation of free radicals that in turn catalyze secondary reactions.

(A) Mass spectrum of extracted cavity sap in the absence of H_2O_2.

(B) Mass spectrum of extracted cavity sap treated with Fenton reagent. In vitro Fenton reactions lead to degradation, especially of the sugar oligomers of DP 4-7.

(C) Detection of oxidized sugar oligomers in control and Fenton reaction samples. After in vitro Fenton reaction, an increased level of the oxidized form $[M-2H+Na]^+$ compared with the nonoxidized sugar oligomers $[M+Na]^+$ was detected.

(D) Summarizing table of detected molecular ions for oligosaccharides and corresponding oxidation products. Presented are the values for sodium adduct ions as being the highest intense sugar signals. Also, for the potassium adduct ions, corresponding oxidized sugars were detected.

ROS are intimately involved in PCD (Apel and Hirt, 2004; Van Breusegem et al., 2008). By the end of the prestorage phase (6 DAP), the NP has become a heterogeneous tissue containing dividing, differentiating, and disintegrating cells. PCD occurs in the part of the NP that faces the endosperm cavity between 6 and 10 DAP (Radchuk et al., 2011), as also shown by the up-regulation of genes related to PCD and protein degradation and an enhanced level of lipoxygenase activity (Thiel et al., 2008). Lipid peroxidation releases H_2O_2, which can then trigger PCD (Van Breusegem and Dat, 2006; Keunen et al., 2013). The identity of the genes activated or upregulated in the barley ETCs over the period 10 to 12 DAP (Thiel et al., 2012) suggests that redox homeostasis occurs during late ETC development when transfer cell architecture is established.

The coincidence of the accumulation of short chain inulin-type fructans with control over ROS homeostasis in the NP and ETCs

suggests an involvement of fructans in the processes that protect these structures from oxidative damage, thereby ensuring an uninterrupted flow of assimilate into the endosperm during the storage phase.

The Direct Participation of Oligosaccharides in ROS Detoxification

Recent experiments have suggested the direct participation of sugars in ROS detoxification (Nishizawa et al., 2008; Peshev et al., 2013; Falkeborg et al., 2014). In tobacco (*Nicotiana tabacum*), enhanced freezing tolerance has been correlated with the increased ROS scavenging capacity generated by the constitutive expression of a bacterial levansucrase gene producing fructans (Parvanova et al., 2004). The protective role for maltose against oxidative stress was demonstrated by the response of *Arabidopsis thaliana* to methyl viologen treatment (Scarpeci and Valle, 2008), while in the same species, photosynthetic efficiency was maintained during drought stress by the increased accumulation of soluble sugars (Moustakas et al., 2011).

Here, the in vitro Fenton reactions applied to the cavity sap showed that particularly DP 4-7 oligosaccharides were susceptible to degradation (Figure 7B). Oxidation of those sugar oligomers has also been observed, as shown by the presence of compounds with a molecular mass reduced by 2 D (Figures 7C and 7D). Although fructan metabolizing enzymes have been extensively studied (Pollock and Cairns, 1991; Van den Ende, 2013), their capacity to produce such products has not been reported to date. The outcome of the in vitro experiment suggests that the presence of oxidized oligosaccharides could be diagnostic for ROS scavenging activity in planta. Prior experiments (Stoyanova et al., 2011) have shown that inulin polysaccharides and 1-kestose are efficient ROS scavenging molecules. Inulin is a more effective scavenger than a number of phenolic compounds (Peshev et al., 2013). It was shown that the different kinds of ROS induce a cleavage of the glycosidic bond, and the degradation of cell wall polysaccharides after ROS exposure has already been described (Fry, 1998; Schweikert et al., 2000; Duan and Kasper, 2011). The interaction of sugars with the hydroxyl radical is thought to involve a hydrogen transfer from a sugar C-H bond, thereby forming water and sugar radicals (Hernandez-Marin and Martínez, 2012). A combination of degradation, recombination and regeneration (e.g., by phenolic compounds) reactions generates stable non radical products (Peshev et al., 2013). Sugar radicals also react with gaseous oxygen (Von Sonntag and Schuchmann, 2001), and in such a reaction an oxidized sugar moiety with a molecular mass reduced by 2 D and the $^{\bullet}$OOH radical are produced. The formation of oxidized oligosaccharides (galactomannans) by $^{\bullet}$OH reactions was reported by Tudella et al. (2011).

In this way, the inulin-type fructans accumulating in the barley endosperm cavity, NP, and ETCs during the storage phase may

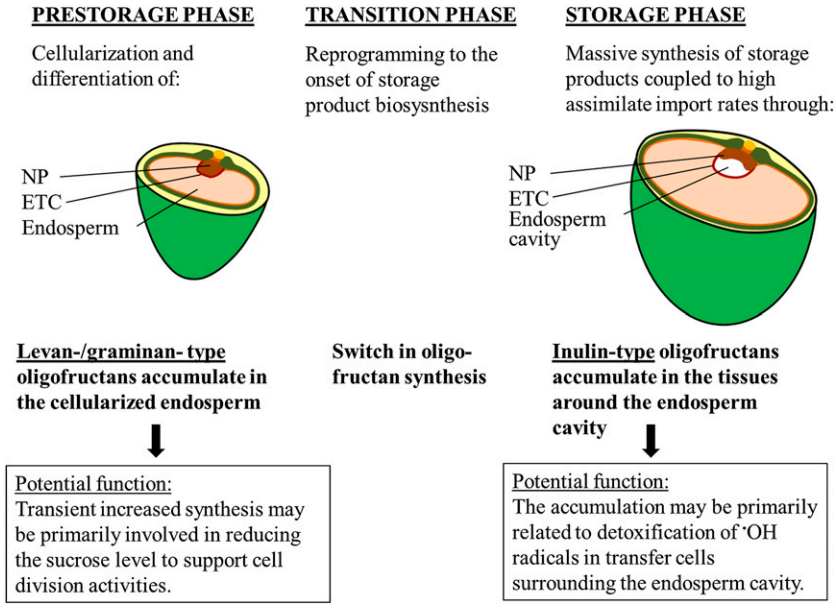

Figure 8. Dynamics of Oligofructan Biosynthesis and the Proposed Functions during Grain Development.

Prior to the onset of starch accumulation in the endosperm, incoming sucrose is transiently stored as levan-/graminan-type fructans. By releasing the glucose moiety during fructan biosynthesis, the high glucose-to-sucrose ratio is preserved. Fructan biosynthesis thereby might contribute to the mechanisms regulating endosperm differentiation in this developmental phase. The transition phase represents a switch in grain fructan metabolism; short-chain inulin-type fructans are biosynthesized in the NP as the endosperm cavity forms and accumulate in the cavity surrounding tissues. The reactivity of oligofructans with the $^{\bullet}$OH radical has been shown in vitro, emphasizing their capability to act as ROS scavenging agents in cells faced with proceedings leading to ROS formation (e.g., the high transport activities in the ETCs and the contiguous degeneration of NP cells directly facing the endosperm cavity). Accumulation of inulins in cells surrounding the cavity might thereby mitigate ROS-inflicted oxidative damage and in turn maintain the massive import rates into the filial grain parts during the storage phase.

contribute to detoxification of hydroxyl radicals. However, a dual role in ROS homeostasis has still to be considered for soluble sugars as particularly sucrose, glucose, and fructose are involved in ROS generation as well as in antioxidant pathways (Couée et al., 2006); for example, sucrose is an important signal triggering defense responses against ROS (Ramel et al., 2007, 2009). In this respect, the conversion of sucrose into short chain inulin-type fructans may help shift the balance in the NP and ETCs toward protection against oxidative stress.

Localization of Inulin-Type Oligofructans

In general, fructans are thought to be localized in the vacuole (Pollock et al., 1996; Vijn and Smeekens, 1999), although an apoplastic localization of fructans and 1-FEH activity was reported (Livingston and Henson, 1998; Kawakami et al., 2005). There are two possible explanations for tissue specificity and unexpected apoplastic localization in developing barley grains. The first is that their high concentration in the cavity sap results from PCD of NP cells. Both Ugalde and Jenner (1990) and Schnyder et al. (1993) have assumed that biosynthesis of oligofructans takes place early in development in the vacuoles of nucellus cells, which consecutively disintegrate. The alternative explanation is that the coexpression of fructan biosynthesis and degradation enzymes is associated with microsome differentiation (Kaeser, 1983; Cairns et al., 2008), which may mediate the export of fructans into the apoplastic cavity (Valluru and Van den Ende, 2008). The simultaneous expression of biosynthetic and degrading enzymes may offer control over the length of the fructan chain to optimize its interaction with the plasma membrane.

The structural flexibility of the sugar rings and glycosidic linkages enables the integration of the sugar molecules between the head groups of the plasma membrane phospholipids (Vereyken et al., 2003; Valluru and Van den Ende, 2008), thereby facilitating the scavenging of ROS close to its site of generation. A positive effect of small DP oligofructans on membrane stability has been demonstrated by in vitro experiments based on liposomes and sugars extracted from oat (*Avena sativa*) and rye (*Secale cereale*) (Hincha et al., 2007). Other investigations have shown a beneficial effect of inulin-type oligofructans on membrane stability under conditions of low temperature or drought stress (Kawakami et al., 2008; Keunen et al., 2013). However, experimental proof for the integration of inulin-type oligofructans into the barley grain ETC plasma membrane remains difficult to establish.

The proposed physiological role of the differential fructan patterns is shown in Figure 8. The biosynthesis of specific oligofructans during grain development is both developmental stage and tissue specific. During the transition phase, a switch in fructan metabolism occurs. The transient accumulation of 6-kestose and bifurcose prior to storage product biosynthesis contributes to balancing the glucose/sucrose ratio that is assumed to prevent a precocious differentiation of the endosperm cells. At the beginning of the storage phase, inulin-type fructans, biosynthesized in the upper part of the NP and probably released into the cavity, may suppress the oxidative stress in the transport active NP and ETCs. The sequestration of short chain oligofructans may represent a highly efficient means of protecting the plasma membrane, thereby maintaining a high rate of assimilate transport.

Experimental proof of such differential oligofructan function during barley grain development, ideally obtained by investigating mutants impaired in fructan metabolism in the distinct tissues, has yet to be provided.

METHODS

Plant Material

Barley (*Hordeum vulgare*) plants were grown in a greenhouse under a 16-h photoperiod (20°C day, 14°C night). *H. vulgare* var Bowman and the corresponding *seg8* mutant were obtained from J.D. Franckowiak (North Dakota State University, Fargo, ND) and grown as described by Weier et al. (2014). Flowers were tagged as described (Weschke et al., 2000), and developing grains were sampled at 3, 7, 10, 14, 17, and 20 DAP. The lemma and palea were removed and the grains snap-frozen in liquid nitrogen and stored at –80°C until required. All experiments were performed in triplicate.

MALDI MSI Sample Preparation

Sample processing involved thin sectioning and the application of a matrix (Peukert et al., 2013). Frozen grains were fixed to the sample holder of a cryotome (cooled to −20°C) using either optimal cutting temperature compound (O.C.T. Tissue-Tek Sakura Finetek Europe) or ice (in the case of very small 3 DAP samples). Longitudinal and cross sections of 30 µm thickness were cut and thaw mounted onto indium tin oxide-coated glass slides (Bruker Daltonics), then dried in a desiccator for 30 min. Prior to matrix application, images were captured with a stereomicroscope (Leica MZ6) connected to a digital camera (AxioCam ICc1; Zeiss).

The matrix was 2,5-dihydroxybenzoic acid (Sigma-Aldrich) diluted to 30 mg/mL in 50% v/v methanol and 0.2% (w/v) trifluoroacetic acid. The matrix was applied using sensor-controlled vibrational vaporization delivered using an ImagePrep device (Bruker Daltonics) according to the manufacturer's instructions.

MALDI Time-of-Flight MSI Measurement

The visualization of metabolites has been facilitated by MSI (Kaspar et al., 2011; Matros and Mock, 2013), while MALDI MSI has allowed for the analysis of certain key molecules with a high level of spatial resolution (Caprioli et al., 1997) and has been proven to be applicable to plant material (Matros and Mock, 2013, and references therein). The MS instrument creates an array of mass spectra, where each spot represents its own *m/z* profile. Gradients of ion abundances were visualized across the sample by a two-dimensional reconstruction of the ion chromatograms. Color coding was used to display the recognition patterns (Gross, 2011). A general overview of the MSI principle is presented in Figure 1C.

The MSI measurements were performed using an ultrafleXtreme MALDI time-of-flight (TOF)/TOF device (Bruker Daltonics) run in positive ionization mode. The instrument was equipped with a Smartbeam-II laser with a repetition rate of 1000 Hz. The laser raster (resolution) was set between 15 and 35 µm depending on the size of the tissue section (for very small sections, a 15-µm laser raster was used). The *m/z* range was set to 80 to 1300 and the sample rate to 0.5 Gs/s. Eight hundred shots per raster spot were acquired with a laser beam width of 10 µm. The acquisition of the laser raster spots was randomly performed in order to eliminate bias due to measurement order. The instrument was calibrated with defined mass signals derived from a polyethylene glycol mixture (1:1 mixture of PEG 200 and 600, diluted 1:300 in 30% v/v acetonitrile and 0.1% w/v trifluoroacetic acid). The programs flexControl v3.3 and flexImaging v.2.1 (Bruker Daltonics) were used to obtain the measurements. The laser power and lateral resolution were selected according to the

needs of each experiment. The acquired single spectra were combined to give an overall average spectrum using flexImaging software (Bruker Daltonics) and further used for the visualization of *m/z* values. The distribution patterns of selected m/z values were displayed in the form of single ion intensity maps.

Tandem mass spectrometry measurements obtained by MALDI TOF/TOF analysis were performed directly on tissue sections using the same instrumentation. Characteristic fragment ions were used for the classification of molecules to a metabolite class.

Sugar Quantitation

Cavity sap was extracted from immature barley grains at 10, 14, 17, and 20 DAP. After snap-freezing, the grains were cut in half, the sap sampled using a microsyringe, and again snap-frozen. Sap samples were heated to 90°C for 5 min to inactivate enzymes. Whole grains were ground with a mortar and pestle. For sugar extraction, 20 volumes (mL/mg) of 1 mM mannitol was added and samples then boiled for 20 min. Samples were centrifuged at 15,000*g* for 10 min. A 200-μL aliquot of the supernatant was laid on a mixed bed Dowex column containing 300 μL each of Dowex H+ and Dowex 1-acetate (Acros Organics) (Van den Ende and Van Laere, 1996). The resins were eluted six times with 200 μL water. Sugar separation was achieved using an anion-exchange HPLC device (Dionex) employing a CarboPac PA100 column, and the outputs quantified by pulsed amperometric detection. Mannitol was used as an internal standard. Peak quantification and identification were performed using an external standards method (Shiomi et al., 1991).

Enzyme Assays

On-Tissue Digestion

Yeast invertase (Sigma Aldrich) was diluted to 0.9 mg/mL (37 units/mL) in 20 mM KH_2PO_4 adjusted with K_2HPO_4 to pH 5. A 400-μL aliquot was injected into the sprayhead of the ImagePrep device (Bruker Daltonics) and applied 50 times sequentially onto a dried tissue section. Each application cycle comprised a 1.5-s period of spraying and a 30-s drying period. As a negative control, 20 mM KH_2PO_4 adjusted with K_2HPO_4 to pH 5 without enzyme was applied in the same way. The material was incubated above a water bath at 55°C for 1 h and subsequently the same matrix was applied as described above. To allow for a direct comparison of signal intensities produced by the MALDI MSI, consecutive slices were used and the treated and control section were measured in random order.

In Vitro Digestion

Cavity sap was extracted from immature barley grains with a micro syringe. Cavity extracts were dissolved in 50 mM potassium acetate (pH 5). The solution was purified by solid phase extraction using TopTip C-18 micro-spin columns (Glygen). The samples were loaded onto equilibrated tips and eluted with 70 μL 10% v/v methanol in 50 mM potassium acetate (pH 5). The eluates were dried and diluted in 50 μL 50 mM potassium acetate (pH 5) prior to enzymatic assays, which were performed in a 20-μL reaction containing 5 μL purified cavity extract, and the respective enzymes: 1-FEH (6 μg/μL, recombinant expressed in *Pichia pastoris*), yeast invertase (2 units; Sigma Aldrich) and α-galactosidase (2 units; MegaZyme). The incubations with invertase and α-galactosidase were performed at 55°C and the ones with 1-FEH at room temperature. As negative controls, incubation mixtures containing heat-inactivated enzyme (5 min, 90°C) or lacking substrate were prepared. Reactions were stopped by heating to 90°C for 5 min. Prior to MALDI TOF mass spectrometry measurement, the samples were repurified through a TopTip C-18 micro-spin column, vacuum-dried, and dissolved in 20 μL 70% v/v methanol. Measurements were performed by MALDI TOF mass spectrometry (ultrafleXtreme; Bruker Daltonics) analyses in positive ionization mode. 2,5-D was used as a matrix (diluted to 30 mg/mL in 50% methanol and 0.2% trifluoroacetic acid).

Quantitative Real-Time PCR

Tissue Preparation for Laser Microdissection and Pressure Catapulting

Frozen grains were transferred to a cryostat kept at −20°C. The central part of the grain was attached to a sample plate using O.C.T. compound. Sections of 20 μm thickness were cut and mounted on PEN membrane slides (PALM) and stored for 7 d at −20°C for dessication. Prior to the LM process, the cryosections were equilibrated at room temperature for 5 min. The LM procedure was performed as described by Thiel et al. (2011).

RNA Processing and qRT-PCR

RNA was extracted from 30 to 50 sections using an Absolutely RNA Nanoprep Kit (Stratagene) and amplified by one round of T7-based mRNA amplification using a MessageAmp aRNA kit (Ambion). The resulting antisense RNA represented the template for first-strand cDNA synthesis, using SuperScript III (Invitrogen) with random priming, according to the manufacturer's instructions. The Power SYBR Green PCR master mix was used to perform the qRT-PCR analyses in an ABI 7900 HT Real-Time PCR system (Applied Biosystems). Data were analyzed using SDS v2.2.1 software (Applied Biosystems). Transcript abundances represented the arithmetic mean of three technical replicates. The chosen reference gene was Hv-Actin1 (AK365182). Dissociation curves confirmed the presence of a single species amplicon in each reaction. The efficiency of each PCR was determined using LinRegPCR software (www.gene-quantification.de/download.html). Values were calculated according to Czechowski et al. (2005) and given as relative expression $((1+E)^{-\Delta Ct})$. A list of primers and their sequences is given in Supplemental Table 4.

Fenton Reagent Compound Reactions

In vitro Fenton reactions were performed on manually extracted cavity sap taken from 14 DAP barley grains, heated for 10 min at 85°C, and then centrifuged for 5 min at 15,000*g*. The reaction mixture consisted of 1 mM H_2O_2, 1 mM ascorbate, 0.1 mM $FeSO_4$, and 0.1 mM EDTA-Na and was allowed to run for 24 h at 30°C. Control samples were treated in the same way without the addition of H_2O_2. Prior to mass spectrometry analysis, each sample was diluted 1:50 in 50% v/v methanol and 0.1% formic acid. As mass spectrometric analysis did not allow the usage of strong ionic buffer, we omitted it in our reaction mixtures. The pH was proven to be neutral after completion of the reaction.

Protein Extraction, Two-Dimensional SDS-PAGE Separation, and Mass Spectrometry Analysis

The samples were ground under liquid nitrogen to a homogenous flour. Aliquots of 100 mg of flour were thawed in 500 μL buffer (5 mM Tris/HCl, pH 7.5, and 1 mM $CaCl_2$) and incubated for 30 min at 4°C on a shaker. After centrifugation (15 min, 4°C), the supernatant was mixed with 4 volumes of ice-cold acetone and incubated at −20°C for 2 h. Proteins were sedimented by centrifugation (5 min, 4°C) and dried afterward in a vacuum centrifuge. The pellet was dissolved in lysis buffer (8 M urea, 2% CHAPS, 20 mM DTT, and 0.5% IPG buffer) by incubating for 1 h at 37°C on a shaker. Insoluble material was pelleted by centrifugation (15 min, room temperature).

Fifty micrograms of protein was loaded by rehydration on 7-cm IPG strips with a pH gradient of 4 to 7. For separation on an IPGphor II unit (GE

Healthcare), the following parameters were used: 14 h rehydration, 30 min gradient to 250 V, 30 min gradient to 500 V, 30 min gradient to 3000 V, and 4.40 h 3000 V with a total of ~15 kVh. After isoelectric focusing, strips were equilibrated for 15 min in 50 mM Tris-HCl, pH 8.8, 6 M urea, 30% v/v glycerin, 2% w/v SDS, 20 mM DTT, and 0.01% bromphenol blue and then placed on top of an 11.25% SDS polyacrylamide gel and covered with 0.5% agarose. After electrophoretic separation gels were washed for 5 min with water and proteins were visualized with Coomassie.

Selected protein spots were manually excised from the two-dimensional electrophoresis gel, digested with trypsin, and subjected to mass spectrometry. Acquisition of peptide mass fingerprint data and corresponding LIFT spectra was performed using an ultrafleXtreme MALDI-TOF device (Bruker Daltonics) equipped with a Smartbeam-II laser with are petition rate of 1000 Hz. The spectra were calibrated using external calibration and subsequent internal mass correction. For databank searching, Biotools 3.2 software (Bruker Daltonics) with the implemented MASCOT search engine (Matrix Science) was used, searching against the barley genome sequences. Search parameters were as follows: monoisotopic mass accuracy; 50 ppm tolerance; fragment tolerance of 0.3 D; missed cleavages 1; and the allowed variable modifications were oxidation (Met), propionamide (Cys), and carbamidomethyl (Cys).

Accession Numbers

Sequence data from this article can be found in the National Center for Biotechnology Information databases under the following accession numbers: AK366020, AK357135, AJ567377, and JQ411252 for *1-SST*; AK354338 and JQ411253 for *1-FFT*; AK253058 and JQ411254 for *6-SFT*; AK252358 for *1-FEH*; and AJ534444 for *6-FEH/CWINV2*.

Supplemental Data

The following materials are available in the online version of this article.

Supplemental Figure 1. Detection of Oligosaccharides in a Barley Grain Section.

Supplemental Figure 2. The Pattern of Sugar Accumulation during Barley Grain Development, as Observed by MALDI MSI Analysis.

Supplemental Figure 3. Enlarged View of Single Ion Intensity Maps for *m/z* 543 and *m/z* 1029.

Supplemental Figure 4. Enzymatic Digestion of Cavity Sap.

Supplemental Figure 5. Identification of 6-SFT out of Two-Dimensional SDS-PAGE Gels.

Supplemental Figure 6. The Pattern of Sugar Accumulation during Grain Development, as Observed by MALDI MSI Analysis of *H. vulgare* var Bowman and *seg8*.

Supplemental Figure 7. ESI-MS/MS Fragmentation of a DP3 Molecular Ion (*m/z* 525.2 $[M-2H+Na]^+$).

Supplemental Table 1. Quantities of Individual Sugars Present in Extracts of the Whole Barley Grain and the Endosperm Cavity.

Supplemental Table 2. Expression Profiles of Genes Involved in Fructan Metabolism in Isolated Barley Grain Tissues.

Supplemental Table 3. Expression Profiles of Genes Involved in Fructan Metabolism in Isolated Barley Grain Tissues of 'Bowman' and *seg8*.

Supplemental Table 4. PCR Primer Sequences Used in qRT-PCR Analyses.

ACKNOWLEDGMENTS

This research was supported by a Deutsche Forschungsgemeinschaft grant (MA 4814/1-1) and by the Leibniz Institute of Plant Genetics and Crop Plant Research. We thank Uta Siebert (IPK-Gatersleben) and Annegret Wolf for their excellent technical assistance and Hans Weber for stimulating discussions.

AUTHOR CONTRIBUTIONS

A.M., M.P., H.-P.M., W.W., and W.V.d.E. designed the research. M.P., J.T., A.M., and D.P. performed the experimental work. M.P., J.T., A.M., and D.P. analyzed the data. M.P., J.T., and A.M. wrote the article.

Received July 18, 2014; revised August 26, 2014; accepted September 8, 2014; published September 30, 2014.

REFERENCES

Andriunas, F.A., Zhang, H.M., Xia, X., Offler, C.E., McCurdy, D.W., and Patrick, J.W. (2012). Reactive oxygen species form part of a regulatory pathway initiating trans-differentiation of epidermal transfer cells in *Vicia faba* cotyledons. J. Exp. Bot. **63:** 3617–3629.

Apel, K., and Hirt, H. (2004). Reactive oxygen species: metabolism, oxidative stress, and signal transduction. Annu. Rev. Plant Biol. **55:** 373–399.

Asthir, B., Duffus, C.M., Smith, R.C., and Spoor, W. (2002). Diamine oxidase is involved in H(2)O(2) production in the chalazal cells during barley grain filling. J. Exp. Bot. **53:** 677–682.

Baguma, Y., Sun, C., Borén, M., Olsson, H., Rosenqvist, S., Mutisya, J., Rubaihayo, P.R., and Jansson, C. (2008). Sugar-mediated semidian oscillation of gene expression in the cassava storage root regulates starch synthesis. Plant Signal. Behav. **3:** 439–445.

Bihmidine, S., Hunter III, C.T., Johns, C.E., Koch, K.E., and Braun, D.M. (2013). Regulation of assimilate import into sink organs: update on molecular drivers of sink strength. Front. Plant Sci. **4:** 177.

Cairns, A.J., Turner, L.B., and Gallagher, J.A. (2008). Ryegrass leaf fructan synthesis is oxygen dependent and abolished by endomembrane inhibitors. New Phytol. **180:** 832–840.

Caprioli, R.M., Farmer, T.B., and Gile, J. (1997). Molecular imaging of biological samples: localization of peptides and proteins using MALDI-TOF MS. Anal. Chem. **69:** 4751–4760.

Cochrane, M.P. (2000). Seed carbohydrates. In Seed Technology and Its Biological Basis, M. Black and J.D. Bewley, eds (Boca Raton, FL: CRC Press), pp. 85–120.

Couée, I., Sulmon, C., Gouesbet, G., and El Amrani, A. (2006). Involvement of soluble sugars in reactive oxygen species balance and responses to oxidative stress in plants. J. Exp. Bot. **57:** 449–459.

Czechowski, T., Stitt, M., Altmann, T., Udvardi, M.K., and Scheible, W.R. (2005). Genome-wide identification and testing of superior reference genes for transcript normalization in Arabidopsis. Plant Physiol. **139:** 5–17.

De Gara, L., de Pinto, M.C., Moliterni, V.M.C., and D'Egidio, M.G. (2003). Redox regulation and storage processes during maturation in kernels of *Triticum durum*. J. Exp. Bot. **54:** 249–258.

Duan, J., and Kasper, D.L. (2011). Oxidative depolymerization of polysaccharides by reactive oxygen/nitrogen species. Glycobiology **21:** 401–409.

Falkeborg, M., Cheong, L.Z., Gianfico, C., Sztukiel, K.M., Kristensen, K., Glasius, M., Xu, X., and Guo, Z. (2014). Alginate oligosaccharides: enzymatic preparation and antioxidant property evaluation. Food Chem. **164:** 185–194.

Felker, F.C., Peterson, D.M., and Nelson, O.E. (1985). Anatomy of immature grains of 8 maternal effect shrunken endosperm barley mutants. Am. J. Bot. **72:** 248–256.

Fenton, H.J.H. (1894). LXXIII.-Oxidation of tartaric acid in presence of iron. J. Chem. Soc. Trans. **65:** 899–910.

Fry, S.C. (1998). Oxidative scission of plant cell wall polysaccharides by ascorbate-induced hydroxyl radicals. Biochem. J. **332:** 507–515.

Gadjev, I., Stone, J.M., and Gechev, T.S. (2008). Programmed cell death in plants: New insights into redox regulation and the role of hydrogen peroxide. In International Review of Cell and Molecular Biology, W.J. Kwang, ed (Waltham, MA: Academic Press), pp. 87–144.

Gross, J.H. (2011). Mass Spectrometry: A Textbook. (Heidelberg, Germany: Springer).

Henry, R., and Saini, H. (1989). Characterization of cereal sugars and oligosaccharides. Cereal Chem. **66:** 362–365.

Hernandez-Marin, E., and Martínez, A. (2012). Carbohydrates and their free radical scavenging capability: a theoretical study. J. Phys. Chem. B **116:** 9668–9675.

Hincha, D.K., Livingston Iii, D.P., Premakumar, R., Zuther, E., Obel, N., Cacela, C., and Heyer, A.G. (2007). Fructans from oat and rye: Composition and effects on membrane stability during drying. Biochim. Biophys. Acta Biomembranes **1768:** 1611–1619.

Housley, T.L., and Pollock, C.J. (1993). The metabolism of fructan in higher plants. In Science and Technology of Fructans, M. Suzuki and N. J. Chatterton, eds (Boca Raton, FL: CRC Press), pp. 191–225.

Ishimaru, T., Hirose, T., Matsuda, T., Goto, A., Takahashi, K., Sasaki, H., Terao, T., Ishii, R., Ohsugi, R., and Yamagishi, T. (2005). Expression patterns of genes encoding carbohydrate-metabolizing enzymes and their relationship to grain filling in rice (*Oryza sativa* L.): comparison of caryopses located at different positions in a panicle. Plant Cell Physiol. **46:** 620–628.

Kaeser, W. (1983). Ultrastructure of storage cells in Jerusalem artichoke tubers (*Helianthus tuberosus* L.) vesicle formation during inulin synthesis. Zeitschrift für Pflanzenphysiologie **111:** 253–260.

Kaspar, S., Weier, D., Weschke, W., Mock, H.P., and Matros, A. (2010). Protein analysis of laser capture micro-dissected tissues revealed cell-type specific biological functions in developing barley grains. Anal. Bioanal. Chem. **398:** 2883–2893.

Kaspar, S., Peukert, M., Svatos, A., Matros, A., and Mock, H.P. (2011). MALDI-imaging mass spectrometry - An emerging technique in plant biology. Proteomics **11:** 1840–1850.

Kawakami, A., Sato, Y., and Yoshida, M. (2008). Genetic engineering of rice capable of synthesizing fructans and enhancing chilling tolerance. J. Exp. Bot. **59:** 793–802.

Kawakami, A., Yoshida, M., and Van den Ende, W. (2005). Molecular cloning and functional analysis of a novel 6&1-FEH from wheat (*Triticum aestivum* L.) preferentially degrading small graminans like bifurcose. Gene **358:** 93–101.

Keunen, E., Peshev, D., Vangronsveld, J., Van den Ende, W., and Cuypers, A. (2013). Plant sugars are crucial players in the oxidative challenge during abiotic stress: extending the traditional concept. Plant Cell Environ.

Koch, K. (2004). Sucrose metabolism: regulatory mechanisms and pivotal roles in sugar sensing and plant development. Curr. Opin. Plant Biol. **7:** 235–246.

Li, Y., Van den Ende, W., and Rolland, F. (2014). Sucrose induction of anthocyanin biosynthesis is mediated by DELLA. Mol. Plant **7:** 570–572.

Livingston III, D.P., Hincha, D.K., and Heyer, A.G. (2009). Fructan and its relationship to abiotic stress tolerance in plants. Cell. Mol. Life Sci. **66:** 2007–2023.

Livingston, D.P., and Henson, C.A. (1998). Apoplastic sugars, fructans, fructan exohydrolase, and invertase in winter oat: Responses to second-phase cold hardening. Plant Physiol. **116:** 403–408.

Lüthje, S., Möller, B., Perrineau, F.C., and Wöltje, K. (2013). Plasma membrane electron pathways and oxidative stress. Antioxid. Redox Signal. **18:** 2163–2183.

Martínez-Noël, G.M., Tognetti, J.A., Salerno, G.L., Wiemken, A., and Pontis, H.G. (2009). Protein phosphatase activity and sucrose-mediated induction of fructan synthesis in wheat. Planta **230:** 1071–1079.

Matros, A., and Mock, H.P. (2013). Mass spectrometry based imaging techniques for spatially resolved analysis of molecules. Front. Plant Sci. **4:** 89.

Melkus, G., et al. (2011). Dynamic $^{13}C/^{1}H$ NMR imaging uncovers sugar allocation in the living seed. Plant Biotechnol. J. **9:** 1022–1037.

Moustakas, M., Sperdouli, I., Kouna, T., Antonopoulou, C.-I., and Therios, I. (2011). Exogenous proline induces soluble sugar accumulation and alleviates drought stress effects on photosystem II functioning of *Arabidopsis thaliana* leaves. Plant Growth Regul. **65:** 315–325.

Nelson, C.J., and Spollen, W.G. (1987). Fructans. Physiol. Plant. **71:** 512–516.

Nishizawa, A., Yabuta, Y., and Shigeoka, S. (2008). Galactinol and raffinose constitute a novel function to protect plants from oxidative damage. Plant Physiol. **147:** 1251–1263.

Offler, C.E., McCurdy, D.W., Patrick, J.W., and Talbot, M.J. (2003). Transfer cells: cells specialized for a special purpose. Annu. Rev. Plant Biol. **54:** 431–454.

Olsen, O.-A. (2001). Endosperm development: Cellularization and cell fate specification. Annu. Rev. Plant Physiol. Plant Mol. Biol. **52:** 233–267.

Parvanova, D., Ivanov, S., Konstantinova, T., Karanov, E., Atanassov, A., Tsvetkov, T., Alexieva, V., and Djilianov, D. (2004). Transgenic tobacco plants accumulating osmolytes show reduced oxidative damage under freezing stress. Plant Physiol. Biochem. **42:** 57–63.

Patrick, J.W., and Offler, C.E. (2001). Compartmentation of transport and transfer events in developing seeds. J. Exp. Bot. **52:** 551–564.

Peshev, D., Vergauwen, R., Moglia, A., Hideg, E., and Van den Ende, W. (2013). Towards understanding vacuolar antioxidant mechanisms: a role for fructans? J. Exp. Bot. **64:** 1025–1038.

Peukert, M., Becker, M., Matros, A., and Mock, H.-P. (2013). Mass spectrometry based imaging of metabolites and proteins. In Plant Proteomics: Methods and Protocols, J.V. Jorrin-Novo, S. Komatsu, W. Weckwerth, and S. Wienkoop, eds (New York: Humana Press), pp. 223–240.

Pollock, C.J., and Cairns, A.J. (1991). Fructan metabolism in grasses and cereals. Annu. Rev. Plant Physiol. Plant Mol. Biol. **42:** 77–101.

Pollock, C.J., and Cairns, A.J. (1999). The integration of sucrose and fructan metabolism in temperate grasses and cereals. In Regulation of Primary Metabolic Pathways in Plants, N.J. Kruger, S.A. Hill, and R.G. Ratcliffe, eds (Dordrecht, The Netherlands: Kluwer Academic Publishers), pp. 195–226.

Pollock, C.J., and Cairns, A.J., Sims, I.M., and Housley, T.L. (1996). Fructans as reserve carbohydrates in crop plants. In Photoassimilate Distribution in Plants and Crops: Source-Sink Relationships, E. Zamski and A.A. Shaffer, eds (New York: Marcel Dekker), pp. 97–114.

Radchuk, V., Weier, D., Radchuk, R., Weschke, W., and Weber, H. (2011). Development of maternal seed tissue in barley is mediated by regulated cell expansion and cell disintegration and coordinated with endosperm growth. J. Exp. Bot. **62:** 1217–1227.

Ramel, F., Sulmon, C., Bogard, M., Couée, I., and Gouesbet, G. (2009). Differential patterns of reactive oxygen species and antioxidative mechanisms during atrazine injury and sucrose-induced tolerance in *Arabidopsis thaliana* plantlets. BMC Plant Biol. **9:** 28.

Ramel, F., Sulmon, C., Cabello-Hurtado, F., Taconnat, L., Martin-Magniette, M.L., Renou, J.P., El Amrani, A., Couée, I., and Gouesbet, G. (2007). Genome-wide interacting effects of sucrose and herbicide-mediated stress in *Arabidopsis thaliana*: novel

insights into atrazine toxicity and sucrose-induced tolerance. BMC Genomics **8:** 450.

Roessner-Tunali, U., Urbanczyk-Wochniak, E., Czechowski, T., Kolbe, A., Willmitzer, L., and Fernie, A.R. (2003). De novo amino acid biosynthesis in potato tubers is regulated by sucrose levels. Plant Physiol. **133:** 683–692.

Rolland, F., Baena-Gonzalez, E., and Sheen, J. (2006). Sugar sensing and signaling in plants: conserved and novel mechanisms. Annu. Rev. Plant Biol. **57:** 675–709.

Rolletschek, H., Weschke, W., Weber, H., Wobus, U., and Borisjuk, L. (2004). Energy state and its control on seed development: starch accumulation is associated with high ATP and steep oxygen gradients within barley grains. J. Exp. Bot. **55:** 1351–1359.

Rolletschek, H., Melkus, G., Grafahrend-Belau, E., Fuchs, J., Heinzel, N., Schreiber, F., Jakob, P.M., and Borisjuk, L. (2011). Combined noninvasive imaging and modeling approaches reveal metabolic compartmentation in the barley endosperm. Plant Cell **23:** 3041–3054.

Scarpeci, T., and Valle, E. (2008). Rearrangement of carbon metabolism in *Arabidopsis thaliana* subjected to oxidative stress condition: an emergency survival strategy. Plant Growth Regul. **54:** 133–142.

Schnyder, H., Gillenberg, C., and Hinz, J. (1993). Fructan contents and dry matter deposition in different tissues of the wheat grain during development. Plant Cell Environ. **16:** 179–187.

Schweikert, C., Liszkay, A., and Schopfer, P. (2000). Scission of polysaccharides by peroxidase-generated hydroxyl radicals. Phytochemistry **53:** 565–570.

Shiomi, N., Onodera, S., Chatterton, N.J., and Harrison, P.A. (1991). Separation of fructooligosaccharide isomers by anion-exchange chromatography (biological chemistry). Agric. Biol. Chem. **55:** 1427–1428.

Sreenivasulu, N., Altschmied, L., Radchuk, V., Gubatz, S., Wobus, U., and Weschke, W. (2004). Transcript profiles and deduced changes of metabolic pathways in maternal and filial tissues of developing barley grains. Plant J. **37:** 539–553.

Stoyanova, S., Geuns, J., Hideg, E., and Van den Ende, W. (2011). The food additives inulin and stevioside counteract oxidative stress. Int. J. Food Sci. Nutr. **62:** 207–214.

Sun, C., Palmqvist, S., Olsson, H., Borén, M., Ahlandsberg, S., and Jansson, C. (2003). A novel WRKY transcription factor, SUSIBA2, participates in sugar signaling in barley by binding to the sugar-responsive elements of the iso1 promoter. Plant Cell **15:** 2076–2092.

Thiel, J., Weier, D., and Weschke, W. (2011). Laser-capture microdissection of developing barley seeds and cDNA array analysis of selected tissues. In Laser Capture Microdissection, G.I. Murray, ed (Totowa, NJ: Humana Press), pp. 461–475.

Thiel, J., Müller, M., Weschke, W., and Weber, H. (2009). Amino acid metabolism at the maternal-filial boundary of young barley seeds: a microdissection-based study. Planta **230:** 205–213.

Thiel, J., Riewe, D., Rutten, T., Melzer, M., Friedel, S., Bollenbeck, F., Weschke, W., and Weber, H. (2012). Differentiation of endosperm transfer cells of barley: a comprehensive analysis at the micro-scale. Plant J. **71:** 639–655.

Thiel, J., Weier, D., Sreenivasulu, N., Strickert, M., Weichert, N., Melzer, M., Czauderna, T., Wobus, U., Weber, H., and Weschke, W. (2008). Different hormonal regulation of cellular differentiation and function in nucellar projection and endosperm transfer cells: a microdissection-based transcriptome study of young barley grains. Plant Physiol. **148:** 1436–1452.

Tudella, J., Nunes, F.M., Paradela, R., Evtuguin, D.V., Domingues, P., Amado, F., Coimbra, M.A., Barros, A.I., and Domingues, M.R. (2011). Oxidation of mannosyl oligosaccharides by hydroxyl radicals as assessed by electrospray mass spectrometry. Carbohydr. Res. **346:** 2603–2611.

Ugalde, T., and Jenner, C. (1990). Substrate gradients and regional patterns of dry matter deposition within developing wheat endosperm. I. Carbohydrates. Funct. Plant Biol. **17:** 377–394.

Valluru, R., and Van den Ende, W. (2008). Plant fructans in stress environments: emerging concepts and future prospects. J. Exp. Bot. **59:** 2905–2916.

Van Breusegem, F., and Dat, J.F. (2006). Reactive oxygen species in plant cell death. Plant Physiol. **141:** 384–390.

Van Breusegem, F., Bailey-Serres, J., and Mittler, R. (2008). Unraveling the tapestry of networks involving reactive oxygen species in plants. Plant Physiol. **147:** 978–984.

Van den Ende, W. (2013). Multifunctional fructans and raffinose family oligosaccharides. Front. Plant Sci. **4:** 247.

Van den Ende, W., and Van Laere, A. (1996). Fructan synthesizing and degrading activities in chicory roots (*Cichorium intybus* L.) during field-growth, storage and forcing. J. Plant Physiol. **149:** 43–50.

Van den Ende, W., and El-Esawe, S.K. (2014). Sucrose signaling pathways leading to fructan and anthocyanin accumulation: a dual function in abiotic and biotic stress responses? Environ. Exp. Bot., in press.

Van den Ende, W., De Coninck, B., and Van Laere, A. (2004). Plant fructan exohydrolases: a role in signaling and defense? Trends Plant Sci. **9:** 523–528.

Vereyken, I.J., van Kuik, J.A., Evers, T.H., Rijken, P.J., and de Kruijff, B. (2003). Structural requirements of the fructan-lipid interaction. Biophys. J. **84:** 3147–3154.

Verspreet, J., Hemdane, S., Dornez, E., Cuyvers, S., Delcour, J.A., and Courtin, C.M. (2013a). Maximizing the concentrations of wheat grain fructans in bread by exploring strategies to prevent their yeast (*Saccharomyces cerevisiae*)-mediated degradation. J. Agric. Food Chem. **61:** 1397–1404.

Verspreet, J., Hemdane, S., Dornez, E., Cuyvers, S., Pollet, A., Delcour, J.A., and Courtin, C.M. (2013b). Analysis of storage and structural carbohydrates in developing wheat (*Triticum aestivum* L.) grains using quantitative analysis and microscopy. J. Agric. Food Chem. **61:** 9251–9259.

Verspreet, J., Cimini, S., Vergauwen, R., Dornez, E., Locato, V., Le Roy, K., De Gara, L., Van den Ende, W., Delcour, J.A., and Courtin, C.M. (2013c). Fructan metabolism in developing wheat (*Triticum aestivum* L.) kernels. Plant Cell Physiol. **54:** 2047–2057.

Vijn, I., and Smeekens, S. (1999). Fructan: more than a reserve carbohydrate? Plant Physiol. **120:** 351–360.

Vilhar, B., Kladnik, A., Blejec, A., Chourey, P.S., and Dermastia, M. (2002). Cytometrical evidence that the loss of seed weight in the miniature1 seed mutant of maize is associated with reduced mitotic activity in the developing endosperm. Plant Physiol. **129:** 23–30.

Von Sonntag, C., and Schuchmann, H.-P. (2001). Carbohydrates. In Radiation Chemistry, Present Status and Future Trends, C.D. Jonah and B.S.M. Rao, eds (Amsterdam: Elsevier), pp. 481–512.

Wang, H.L., Offler, C.E., and Patrick, J.W. (1995a). The cellular pathway of photosynthate transfer in the developing wheat grain. II. A structural analysis and histochemical studies of the pathway from the crease phloem to the endosperm cavity. Plant Cell Environ. **18:** 373–388.

Weber, H., Borisjuk, L., and Wobus, U. (1997). Sugar import and metabolism during seed development. Trends Plant Sci. **2:** 169–174.

Weber, H., Borisjuk, L., and Wobus, U. (2005). Molecular physiology of legume seed development. Annu. Rev. Plant Biol. **56:** 253–279.

Weier, D., Thiel, J., Kohl, S., Tarkowská, D., Strnad, M., Schaarschmidt, S., Weschke, W., Weber, H., and Hause, B. (2014). Gibberellin-to-abscisic

acid balances govern development and differentiation of the nucellar projection of barley grains. J. Exp. Bot. **65:** 5291–5304.

Weschke, W., Panitz, R., Sauer, N., Wang, Q., Neubohn, B., Weber, H., and Wobus, U. (2000). Sucrose transport into barley seeds: molecular characterization of two transporters and implications for seed development and starch accumulation. Plant J. **21:** 455–467.

Weschke, W., Panitz, R., Gubatz, S., Wang, Q., Radchuk, R., Weber, H., and Wobus, U. (2003). The role of invertases and hexose transporters in controlling sugar ratios in maternal and filial tissues of barley caryopses during early development. Plant J. **33:** 395–411.

Wind, J., Smeekens, S., and Hanson, J. (2010). Sucrose: metabolite and signaling molecule. Phytochemistry **71:** 1610–1614.

Wobus, U., Sreenivasulu, N., Borisjuk, L., Rolletschek, H., Panitz, R., Gubatz, S., and Weschke, W. (2005). Molecular physiology and genomics of developing barley grains. Recent Res. Dev. Plant Mol. Biol. **2:** 1–29.

Zhou, Y., Andriunas, F., Offler, C.E., McCurdy, D.W., and Patrick, J.W. (2010). An epidermal-specific ethylene signal cascade regulates trans-differentiation of transfer cells in *Vicia faba* cotyledons. New Phytol. **185:** 931–943.